Journal of African Earth Sciences 129 (2017) 898–909

Contents lists available at ScienceDirect

Journal of African Earth Sciences

journal homepage: www.elsevier.com/locate/jafrearsci

# Lithology, petrography and Cu occurrence of the Neoproterozoic glacial Mwale Formation at the Shanika syncline (Tenke Fungurume, Congo Copperbelt; Democratic Republic of Congo)

Pascal Mambwe [a, b, c], Luke Milan [d], Jacques Batumike [a, e, *], Sébastien Lavoie [b], Michel Jébrak [f], Louis Kipata [a], Mumba Chabu [a], Sonya Mulongo [a], Toto Lubala [a], Damien Delvaux [g], Philippe Muchez [c]

[a] Department of Geology, University of Lubumbashi, B.P.1825, Lubumbashi, Congo
[b] Department of Exploration Geology, Tenke Fungurume Mining S.A., Route de l'Aéroport, Batiment TFM, Commune Annexe, Lubumbashi, Congo
[c] KU Leuven, Department of Earth and Environmental Sciences, Celestijnenlaan 200E, B-3001 Leuven, Belgium
[d] Division of Earth Sciences, School of Environmental and Rural Science, University of New England, Armidale, NSW 2351, Australia
[e] Australian Research Council Centre of Excellence for Core to Crust Fluid Systems (CCFS) and GEMOC, Department of Earth and Planetary Sciences, Macquarie University, NSW 2109, Australia
[f] Department of Earth Science and Atmosphere, University of Quebec, Montreal, Canada
[g] Department of Geology and Mineralogy, Royal Museum for Central Africa (RMCA), Leuvensesteenweg 13, 3080 Tervuren, Belgium

ARTICLE INFO

*Article history:*
Received 1 September 2016
Received in revised form
10 February 2017
Accepted 13 February 2017
Available online 15 February 2017

*Keywords:*
Mwale Formation
Congo copperbelt
Neoproterozoic glaciation
Cu sulphide mineralisation
Hydrothermal chlorite

ABSTRACT

The Mwale Formation that constitutes the base of the Nguba Group in the Neoproterozoic Katanga Supergroup has recently attracted renewed interest for copper mineral exploration. We present new field observations combined with detailed logging and petrography of MWAS0001 drill hole at Shanika syncline in the Tenke Fungurume Mining District. Our study has enabled us to subdivide the Mwale Formation into 7 distinct sequences. This succession is host to glaciogenic, glaciomarine, glaciofluvial and glaciolacustrine deposits. Glaciomarine beds are typically a deposit by debris flow in deep water marine environment, induced by basin wide tectonics and glaciation influence. Glaciofluvial beds were deposited in shallow water, fluvial deltaic environment. The glaciolacustrine environment is indicated by dropstones occurring in the laminated mudstone and rhythmites with dispersed clasts observed in the siltstone and conglomerate. These beds are interlayered within the glaciogenic beds, and are characterised by variable clast composition (felsic, mafic and metamorphic). The clasts are very poorly sorted, angular, rounded to moderately rounded, faceted or striated, and supported in a sandy argillaceous or mud matrix.

Two main episodes of sulphide mineralisation are distinguished in the Mwale Formation. The diagenetic episode consists of disseminated euhedral and framboidal pyrites. The hydrothermal episode is associated with Mg-metasomatism and characterised by low grade copper mineralisation that occurs (i) in veins filled with carbonate-chlorite and carbonate-quartz-chlorite-Cu sulphides, such as chalcocite, chalcopyrite and bornite, and (ii) as disseminated sulphides within the host rock. This second episode is late to post-orogenic and can be correlated with late brittle tectonics within the Lufilian arc. The other alteration types include silicification and potassic alteration; however, these alterations are not associated with mineralisation.



## 1. Introduction

The Congo Copperbelt in the central part of Africa (Fig. 1) is known for its world class Cu-Co and Cu-Pb-Zn mineralisation hosted within different stratigraphic levels of the Katanga Supergroup (Cailteux et al., 2005; De Waele et al., 2006; Haest and

* Corresponding author. ARC Centre of Excellence for Core to Crust Fluid Systems and GEMOC ARC National Key Centre, Earth and Planetary Sciences, Faculty of Science and Engineering, Macquarie University, NSW 2109, Australia. Tel.: +61 432 370 677; fax: +61 2 9850 8943.
*E-mail address:* jacques.batumike@mq.edu.au (J. Batumike).

http://dx.doi.org/10.1016/j.jafrearsci.2017.02.021
1464-343X/

Muchez, 2011; Hitzman et al., 2012). Most of the Cu-Co deposits in the Congo Copperbelt are hosted within the lower part of the Roan Group. Thus, extensive exploration activities within the copperbelt focussed on the Roan Group. Both Nguba and Kundelungu Groups are still less explored although during the last five years some Cu-(Zn-Pb) mineralisations were discovered within them. The discovery of the Kamoa deposit (Broughton and Rogers, 2010) located approximately 25 km west of the Kolwezi Mining District, where Cu mineralisation is hosted in the diamictite (Mwale Formation-Ng1.1, Table 1), has induced interest for the Nguba Group rocks. Similar style of mineralisation is also found at the Fishtie deposit in central north Zambia (Hendrickson et al., 2015) and at the Tenke Fungurume Mining District (TFMD), one of the largest Cu-Co mining districts in the Congo Copperbelt in the south-eastern part of the Democratic Republic of Congo (DRC) (Schuh et al., 2012).

Most of the previous studies on the Katanga Supergroup diamictites focussed on detailed lithology, geochronology, stratigraphy, and very few on ore petrology (Batumike et al., 2006; Binda and Van Eden, 1972; François, 1973; Hendrickson et al., 2015; Key et al., 2001; Master et al., 2005; Master and Wendorff, 2011; Schmandt et al., 2013). Glaciogenic and glaciomarine deposits are interpreted as the main characteristic of the Mwale Formation in the Congo-Zambia Copperbelt, but they are also described in other Neoproterozoic diamictites such as in the West Congolian belt in the western part of DRC (Delpomdor et al., 2016), the Chuos Formation in Namibia (Le Heron et al., 2013), the Granville Formation in France and the Gaskiers Formation in Canada (Eyles, 1990), the Atud diamictite in Egypt and the Nuwaybah diamictite in Saudi Arabia (Ali et al., 2010). Glaciofluvial deposits characterised by continental glaciation were mentioned in the northern part of the Congo Copperbelt (Wendorff and Key, 2009).

A recent exploration drill hole (MWAS0001) in the central part of the TFMD intercepted the Mwale Formation, revealing previously unrecognised lithological succession and interesting Cu mineralisation. This Cu mineralisation is hosted within a particular lithostratigraphic succession not recognised before in the Katanga Supergroup. The identified sequences include glaciogenic, glaciomarine, glaciofluvial and glaciolacustrine units. Based on petrography, sedimentology and mineralogy, the aims of this paper are: (i) to describe the different facies of the diamictite and their relationship with Cu mineralisation, (ii) to discuss the depositional model of the diamictite, and (iii) to investigate the origin of Cu mineralisation and its spatial distribution.

## 2. Geological setting

The Katanga Supergroup in the central part of Africa extends from the northern part of Zambia to the southeastern part of DRC. This Supergroup is ~10 km-thick and commonly subdivided into three groups based on the presence of two regional diamictites: Roan (R), Nguba (Ng) and Kundelungu (Ku) groups from bottom to the top (Table 1; Batumike et al., 2007a; François, 1973). The two regional diamictites represent two worldwide glacial events during the Neoproterozoic time (Goddéris et al., 2003; Hoffman et al., 1998; Young, 2002). The older diamictite named Grand Conglomérat or Mwale Formation (~720 Ma) can be correlated with the

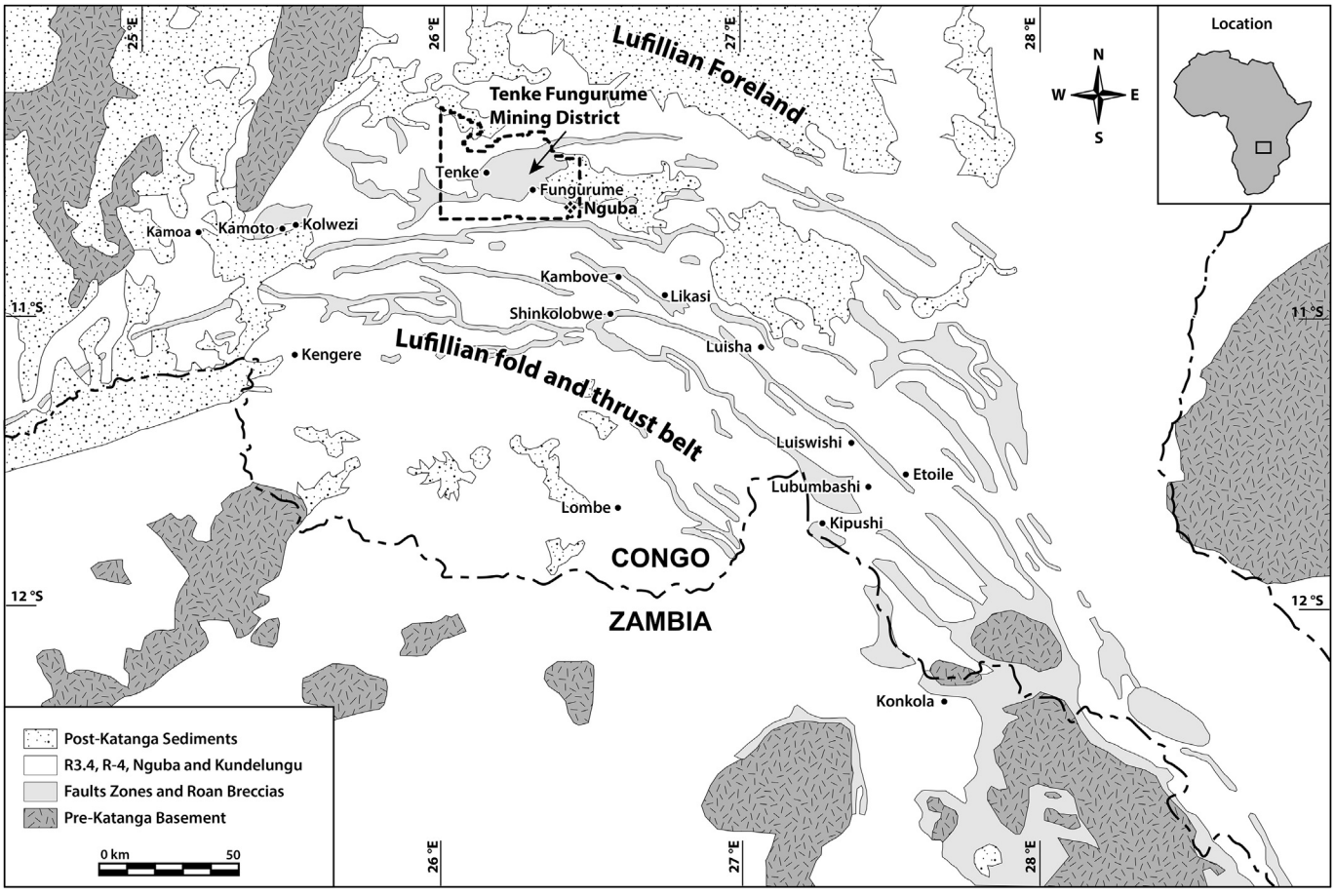


**Fig. 1.** Location of the Tenke Fungurume Mining District within the Congo copperbelt.

**Table 1**
Lithostratigraphy of the Neoproterozoic Katanga Supergroup (Cailteux et al., 1994, 2007; Batumike et al., 2007a) including ages from Hanson et al. (1993), Armstrong et al. (2005), Master et al. (2005) and Graham et al. (2016).

| Supergroup | Ages | Group | Subgroup | Formation | Members & lithologies |
|---|---|---|---|---|---|
| Katanga | ~570 Ma | Kundelungu Ku | Biano Ku 3 | | Arkoses, conglomerates, argillaceous sandstones, sedimentary breccias |
| | | | Ngule Ku 2 | Sampwe - Ku 2.3 | Dolomitic pelites, argillaceous to sandy siltstones |
| | | | | Kiubo - Ku 2.2 | Dolomitic sandstones, siltstones and pelites |
| | | | | Mongwe - Ku 2.1 | Dolomitic pelites, siltstones, sandstones and sedimentary breccias |
| | | | | Lubudi - Ku 1.4 | Pink oolitic limestone |
| | | | Gombela Ku 1 | Kanianga - Ku 1.3 | Carbonate siltstones, shales and sedimentary breccias |
| | | | | Lusele - Ku 1.2 | Pink to grey micritic dolomite (Calcaire Rose) |
| | ~635Ma | | | Kiandamu - Ku 1.1 | Petit Conglomérat tillite/diamictite |
| | | | Bunkeya Ng 2 | Monwezi - Ng 2 | Dolomitic sandstones, siltstones and pelites |
| | | | | Katete - Ng 2.1 | Dolomitic sandstones or siltstones in northern facies; alternating shale and dolomite beds ("Série Récurrente") in southern facies |
| | | Nguba Ng | | Kipushi - Ng 1.4 | Dolomite with dolomitic shale beds |
| | | | Muombe Ng 1 | Kakontwe - Ng 1.3 | Carbonates |
| | | | | Kaponda - Ng 1.2 | Carbonate shales and siltstones; dolomie Tigrée at the base |
| | ~720 Ma | | | Mwale - Ng 1.1 | Grand Conglomérat tillite/diamictite |
| | | | Mwashya (formerly Upper Mwashya) R 4 | Kanzadi - R 4.3 | Sandstones or alternating siltstones and shales |
| | | | | Kafubu - R 4.2 | Carbonaceous shales |
| | | | | Kamoya - R 4.1 | Dolomitic shales, siltstones, sandstones, including conglomeratic beds and cherts in variable position |
| | | | | Kansuki - R 3.4 | Dolomites including volcaniclastic beds (formerly Lower Mwashya) |
| | | | | Mofya - R 3.3 | Dolomites, arenitic dolomites, dolomitic siltstones |
| | | | Dipeta R 3 | R 3.2 | Argillaceous to dolomitic siltstones with interbedded feldspathic sandstones or white dolomites; intrusive gabbros |
| | | Roan R | | RGS - R 3.1 | Argillaceous dolomitic siltstones (R.G.S., "Roches Gréso-Schisteuses") |
| | | | | Kambove - R 2.3 | stromatolitic, laminated, shaly or talcose dolomites; locally sandstones at base; beds of siltstones at top |
| | | | Mines R 2 | Shales Dolomitiques - R 2.2 | Dolomitic shales including three carbonaceous horizons; occasional dolomites |
| | | | | Kamoto - R 2.1 | Stromatolitic dolomite (R.S.C.), silicified/arenitic dolomites (R.S.F./D.Strat.), grey argillaceous dolomitic siltstone at the base (Grey R.A.T.) |
| | 833 ± 10 Ma | | R.A.T. R 1 | | Red argillaceous dolomitic siltstones and sandstones ("Roches Argilo-Talqueuses") |
| | | | Base of the R.A.T. sequence unknown | | |
| | <900 Ma | | | | Basal conglomerate |

Sturtian glaciation and the younger Petit Conglomérat or Kyandamu Formation (~635 Ma) can be correlated with the Marinoan glaciation (Armstrong et al., 2005; Batumike et al., 2006, 2007a; Cailteux et al., 2007; François, 1973; Graham et al., 2016; Key et al., 2001; Master and Wendorff, 2011). The presence of these Neoproterozoic diamictites overlain by cap carbonates is considered as evidence for global icehouse periods (snowball earth) during the Cryogenian (Boyle et al., 2007; Hoffman and Schrag, 2002; Hoffman et al., 1998), but diamictites can also reflect deep-water deposition with both tectonic and indirect glacial influences (Delpomdor et al., 2016; Eyles and Januszczak, 2004). Detrital zircons from the Mwale formation present a large population of Paleoproterozoic age and minor populations of Mesoproterozoic and Archean ages (Batumike et al., 2007b; Master et al., 2005). This suggests that the Congo craton, the Bangweulu block, the Kibara belt, the Irumide belt and the Choma Kalomo block supplied sediments in the Katanga basin (Batumike et al., 2007b; Hanson et al., 1993; Master et al., 2005).

The Roan Group consists of clastic sedimentary rocks and carbonates, mainly dolomites and dolomitic shales (Cailteux, 1994; François, 1987; Oosterbosch, 1962). The Roan sediments were deposited in a basin that evolved from a continental rift to a proto-oceanic (Afar/Red Sea type) rift linked to the breakup of the Rodinia supercontinent (Kampunzu et al., 2000; Meert and Van der Voo, 1997; Tembo et al., 1999). The Mwashya Subgroup at the top of Roan Group (Cailteux et al., 2007) and the overlying Nguba and Kundelungu Groups form thick carbonate and siliciclastic sequences that were deposited in a wider basin corresponding to a major phase of extensional tectonics and normal faulting that marked the transition to a Red Sea-type proto-ocean (Buffard, 1988; Kampunzu et al., 1993).

The Katanga Supergroup sediments were affected by the Lufilian orogeny that operated through three major tectonic phases (Kampunzu and Cailteux, 1999). The first phase (D1) or Kolwezian phase was a northward verging folding and thrusting event which is considered to be coeval to the main deformation phase within the Zambezi belt. The second phase (D2) or Monwezian phase was characterised by large left-lateral strike-slip faults. The third phase (D3) or Shilatembo phase was marked by compressional structures transverse to the NW general trend of the belt. The Lufilian orogeny produced two contrasting domains, fold and thrust belt to the south named Lufilian arc, and the tabular Katangan aulacogen or foreland to the north (Fig. 1). This tectonic model was detailed by a fault kinematic analysis and palaeostress inversion that revealed a total of eight brittle deformation stages, from the peak of the Lufilian orogeny to the East African rifting (Kipata et al., 2013).

Cailteux et al. (2005), De Waele et al. (2006), El Desouky et al. (2009), Haest and Muchez (2011) and Selley et al. (2005) proposed a multistage model for the origin of the Cu-Co mineralisation in the copperbelt. Supergene alteration of Cu-Co minerals and late remobilisation of mineralisation are common phenomenon in the upper oxidation zone (Batumike et al., under review; Cailteux et al., 2005; De Putter et al., 2010; De Waele et al., 2006; El Desouky et al., 2010; François, 2006; Taylor et al., 2013). In the Katangan foreland (Fig. 1), El Desouky et al. (2008) postulated a post-orogenic fluid–mixing model controlled by strike-slip faults. Muchez et al. (2008) and Van Wilderode et al. (2013, 2014, 2015) used Sr and Nd isotopes to characterise the Cu-Co mineralising fluid in several deposits in the copperbelt. According to these authors, the mineralising fluid had interacted with basement rocks of mafic and felsic composition, and siliciclastic sedimentary rocks.

The Shanika syncline in the central part of the TFMD contains mostly the rocks belonging to the Nguba Group, Mwashya Subgroup and Kansuki Formation (Figs. 2 and 3). This package that overlies the Dipeta Subgroup through an unconformity is defined as a klippe (François, 2006; Schuh et al., 2012). Three small Cu-Co mineralised tectonic sheets of the Mines Subgroup occur to the south of the Shanika syncline along an E-W fault. The structural

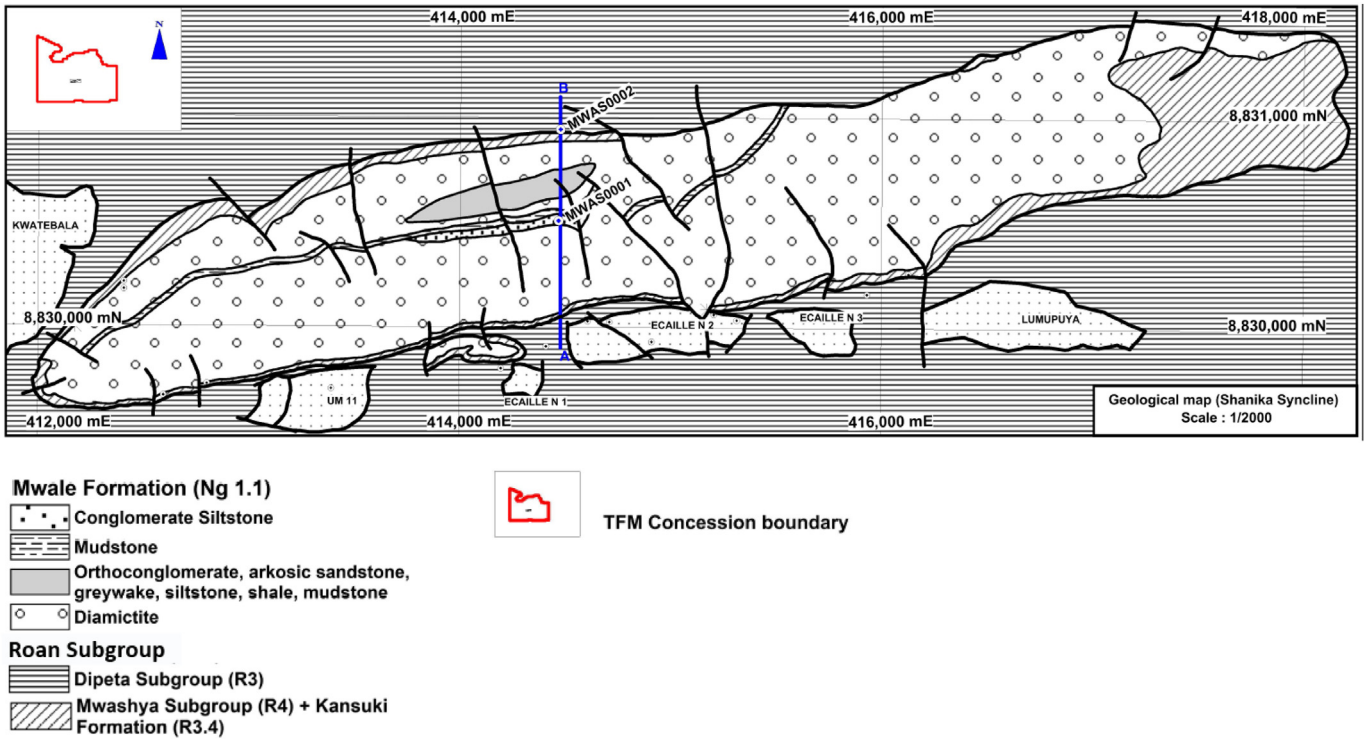


**Fig. 2.** Location of drill holes MWAS001 and MWAS002 in the Shanika syncline.

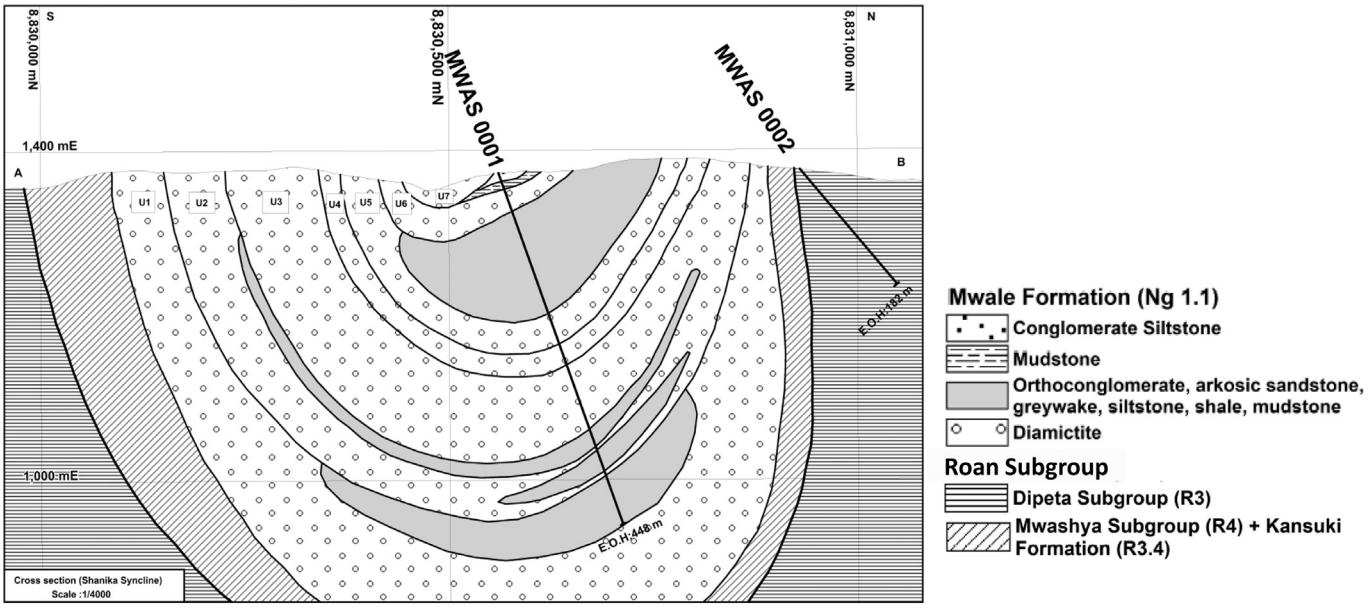


**Fig. 3.** Cross-section showing the stratigraphic succession in the Shanika syncline.

aspects of Katanga Supergroup rocks in the TFMD reflect the main tectonic phases that affected the Lufilian arc (François, 1987, 2006; Jackson et al., 2003; Kampunzu and Cailteux, 1999; Kipata et al., 2013).

## 3. Methods

The lithostratigraphical succession presented in this paper is based on field observations at the Shanika syncline, detailed logging of two drill holes (MWAS0001 and MWAS0002) and macroscopic description of rocks in the Tenke Fungurume concession. Representative samples of each lithological unit from the drill hole MWAS0001 were collected for a petrographic study. Thin sections were prepared at the University of New England and a detailed microscopic description was done on Leica dm750p model petrographic microscope. Modal composition of the rocks was determined by counting statistics on outcrops and drill core. On half drill cores, clasts were measured on sections of 1 or 2 m interval and converted to volume. On thin sections, the modal composition was determined visually using the standard diagrams

**Table 2**
Summary of lithologies, structures, mineralisation and depositional environment of the Mwale Formation in the Shanika syncline.

| MWAS0001 (Depths in meter) | Unit (Thickness in meter) | Lithologies and sedimentological characteristics | Ore minerals | Deposition |
|---|---|---|---|---|
| Not intercepted by drilling | **U7** >20 m | Diamictite with argillaceous matrix | | Glaciogenic |
| 00.00–2.800 | **U6** | Soil | | |
| 2.80–10.82 | ~52 m | Siltstone conglomerate. Rhythmites with dispersed clasts | | Glaciolacustrine |
| 10.82–20.60 | | Mudstone with dropstone | | |
| 20.60–68.30 | | Diamictite with massive and finely laminated argillaceous matrix. Greywacke and shale beds. | Pyrite associated with chlorite. | Glaciogenic |
| 68.30–180.00 | **U5** 30 - 160 m | Orthoconglomerate, arkosic sandstone, siltstone and shale. Cross bedding, erosional surfaces, load deformation, groove and roll marks. | Pyrite, chalcopyrite, bornite associated with chlorite | Glaciofluvial |
| 180.00–225.50 | | Diamictite with sandy argillaceous matrix. | Pyrite and chalcopyrite associated with chlorite | Glaciogenic |
| 225.50–242.40 | **U4** ~22 m | Diamictite with laminated argillaceous sandy matrix and Lithic greywacke with greywacke beds. | Pyrite associated with chlorite. | |
| 242.40–330.60 | **U3** 40 -110 m | Diamictite with sandy argillaceous and argillaceous matrix and greywacke beds | Pyrite, chalcopyrite, bornite associated with chlorite | |
| 330.60–356.15 | **U2** 20 - 80 m | Orthoconglomerate, arkosic sandstone, siltstone and shale. Neptunian dykes and sill injections. Bouma sequences, slumps, groove marks and erosional surfaces. | Pyrite and chalcopyrite associated with chlorite | Glaciomarine |
| 356.15–356.55 | | Diamictite with sandy massive matrix | Pyrite, chalcopyrite, chalcocite associated with chlorite | Glaciogenic |
| 356.55–380.40 | | Orthoconglomerate, arkosic sandstone, siltstone and shale. Slumps and erosional surfaces. | | Glaciomarine |
| 380.40–383.80 | | Diamictite with sandy massive matrix | | Glaciogenic |
| 383.80–448.00 | **U1** | Orthoconglomerate, arkosic sandstone, siltstone and shale. | Pyrite and chalcopyrite | Glaciomarine |
| **E.O.H** | >200 m | Sill injections, slumps, groove, roll and flute marks | associated with chlorite | |
| Not intercepted by the drilling | | Diamictite with argillaceous matrix | | Glaciogenic |
| Not intercepted by the drilling | Kansuki Formation (R3.4) and the Mwashya Subgroup (R4) | | | |

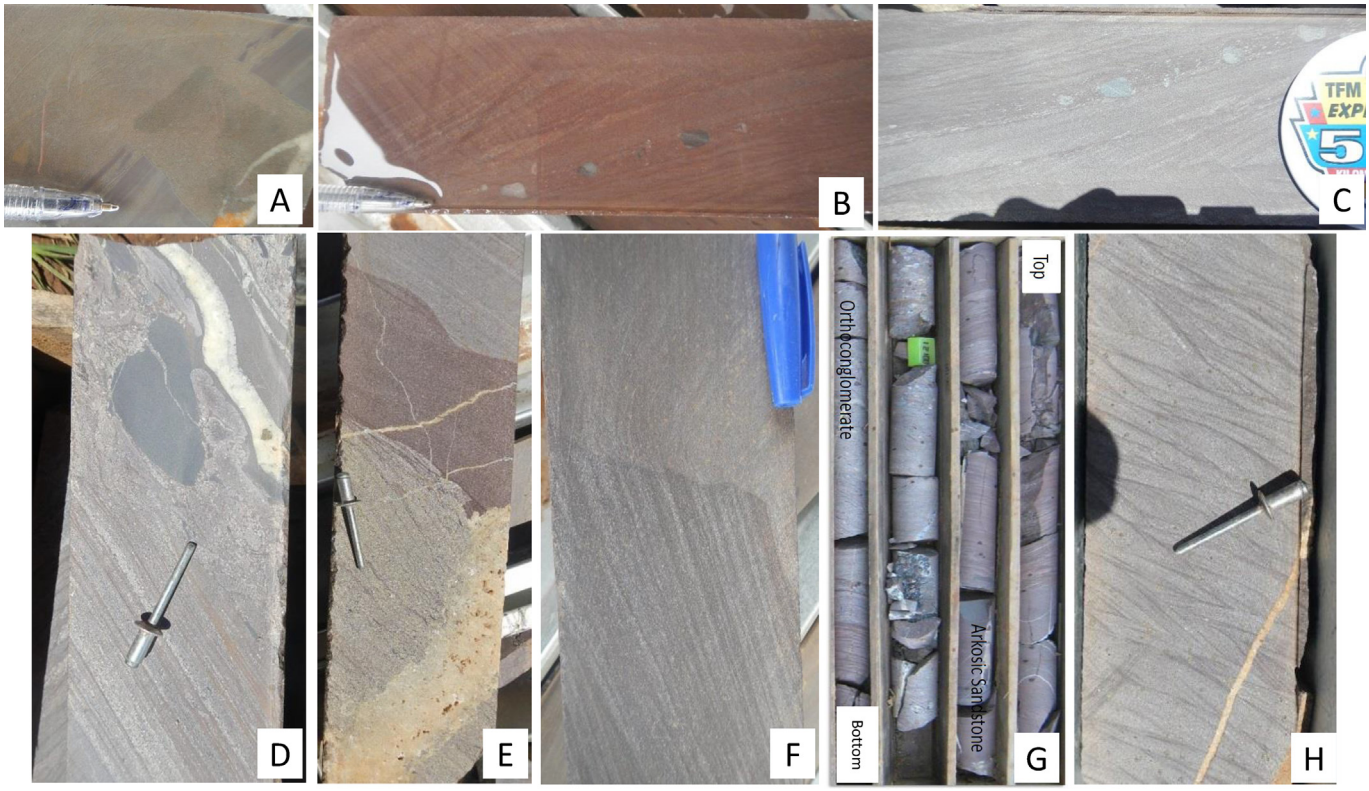


**Fig. 4.** Sedimentary structures and soft sediment deformation structures: (A) Neptunian dykes per descensum and sills by injection shales; (B) and (C) Scour and toll mark, (D) Balls and pillows structure, (E) Load structure, (F) Erosional surface, (G) Bouma sequence; (H) Cross bedding in arkosic sandstone.

of Terry and Chillingar (Berkman, 2001). The lithostratigraphical subdivision was based on the occurrence of different sedimentary facies within the glacial, marine, fluvial and lacustrine deposits constituting the Mwale Formation.

## 4. Stratigraphy and petrography

Drill hole MWAS0001 intercepted only the Mwale Formation. The description of the Mwashya Subgroup (R4) and Kasunki Formation (R 3.4) are based on the field observations as these rocks crop out in the Shanika syncline (Fig. 2). The Kansuki Formation (formerly Lower Mwashya, Table 1) consists of siliceous dolomite with hematite and dolomite veins, oolitic dolomite and banded iron beds. The Mwashya Subgroup (formerly Upper Mwashya, Table 1) is represented by the Kamoya Formation (R 4.1) consisting of sandstones and shales. The Dipeta Subgroup (R3) was intercepted by the MWAS0002 drill hole but also crops out in the Shanika syncline. Its lithologies consist, from bottom to top, of massive dolomite, calcareous dolomite and laminated talc-rich dolomite (Fig. 3).

Seven different units were identified within the Mwale Formation based on lithology (mainly the presence of diamictite layers), petrography and sedimentary features (Table 2). The contact between the Mwale Formation and the underlying Mwashya Subgroup is characterised by an erosional surface.

Unit 1 (U1, up to 200 m thick) at the base, consists of a diamictite, which is overlain by alternating massive conglomerate, fine-to coarse-grained sandstone, thin-to thick-bedded siltstone, laminated and thinly-bedded mudstone. The lower beds of this diamictite were not intercepted by the MWAS0001 drill hole, but were observed on outcrop (Figs. 2 and 3). The thickness of this diamictite layer varies from 25 to 120 m and the clasts are poorly sorted in a massive argillaceous matrix. Clasts include quartz and quartzite (62–85 vol %), dolomite (5–10 vol %), sandy dolomite with hematite spots (3–10 vol %), granite (3–5 vol %), shale (2–5 vol %), micaschist (1.5–4 vol %), jasper (0.5–1 vol %), sandstone (0.5–1 vol %) and oolitic dolomite (0.5 vol %).

The conglomerate can be classified texturally as an orthoconglomerate. It is made up of poorly sorted clasts of quartzite, sandstone and stratified or massive siliceous dolomite within a sandy matrix. Coarse-grained quartz is more abundant than fine-grained quartz in the matrix. The massive sandstone (10 m thick) consists of angular to subrounded quartz grains, minor biotite and weathered orthoclase. Siltstone beds (1–1.20 cm thick) with local fine laminations are interlayered with laminated mudstone (1–10 cm thick).

Soft Sediment Deformation Structures identified within Unit 1 include neptunian dykes and injection structures (Fig. 4a). Erosional surfaces, grooves, bounce marks, roll marks and flute marks are common in the mudstone and siltstone beds (Fig. 4b and c). Load structures including balls and pillow structures can be observed at the contact between massive sandstone and the underlying laminated mudstone beds (Fig. 4d). Locally, some sandstone sill injections and slump structures are observed in the bedded mudstones. The sedimentary structures recognised in the upper beds of U1 are typical of a gravity flow deposition in deep water.

Unit 2 (U2, 81 m thick) is constituted of a 45 m-thick diamictite overlain by two sets of orthoconglomerate, sandstone, siltstone and mudstone beds. These sets have different thicknesses; the first set is 26 m thick and the second 10 m thick. This succession was also described at the Mamfwe anticline, north of the Kimweulu syncline (Cailteux, 1991). Erosional surfaces and grooves are common at the contact between siltstone and laminated mudstone. Detailed examination of samples suggests that there is no significant change in the petrography of the orthoconglomerate, sandstone, siltstone and

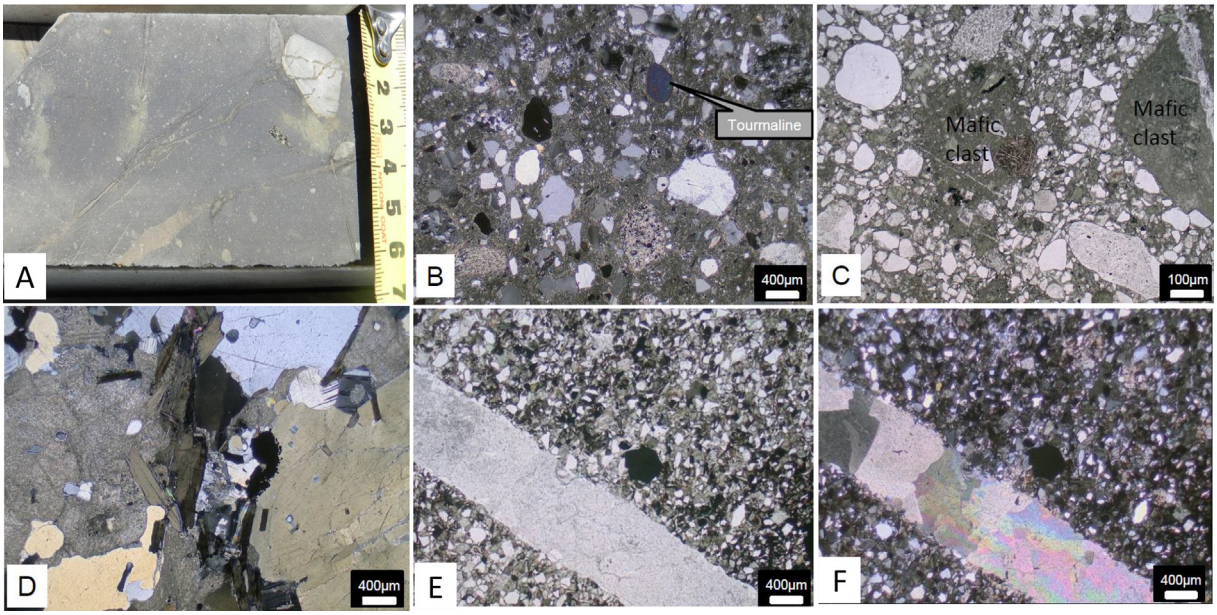


**Fig. 5.** Host-rock petrography: (A) Diamictite, (B) Lithic greywacke with large rounded tourmaline, (C) Lithic clasts of mafic volcanics, and quartzite and fine grained siltstones, (D) Large pebble (10 cm) of a granitic orthogneiss. This rock shows a gneissic foliation. (E) Arkose nature of the mineralised host-rock. Note the vein and large euhedral pyrite (opaque), PPL (F) Same section in XPL.

mudstone from U2 and U1. Locally the succession illustrates a Bouma-type sedimentary sequence. Bouma-type sequence and the deposition of the orthoconglomerate through shearing on the sandstone are characteristic of a turbidite deposit (e.g., Shanmugam, 1997). The diamictite includes striated and faceted, rounded to subrounded clasts of quartzite (60 vol %), granite (15 vol %), siltstone (10 vol %), sandstone (5 vol %), quartz (5 vol %) and orthoclase (4 vol %) in a greenish grey massive sandy matrix.

Unit 3 (U3, 110 m thick) is a greenish grey to black diamictite with an argillaceous to sandy massive matrix. The clasts include quartzite (20–40 vol %), sandstone (15–20 vol %), granite (5 vol %), micaschist (5 vol %), shale (4–5 vol %), siliceous dolomite (0.5–1 vol %), jasper (0.5–1 vol %) and gneiss (1 vol %). Most of the clasts are rounded with few subrounded to angular or striated clasts. The diamictite also includes greywacke beds with localised graded bedding (up to 13 cm thick), argillaceous laminated mudstone beds (up to 35 cm thick) and siltstone beds (up to 30 cm thick). Erosional surfaces similar to those described in U2 are also observed within this diamictite, especially at the contact with the greywacke beds. Chloritisation is more pronounced in greywacke beds especially where graded beddings are observed. On thin section, the greywacke is very similar to the diamictite described above but the greywacke matrix is far less than 15 vol % and mono-mineralic quartz grains are abundant.

Unit 4 (U4, 22 m thick) is a chlorite-rich diamictite with a laminated argillaceous sandy matrix. It contains abundant pyrite, and locally the matrix becomes massive argillaceous or sandy (Fig. 5a). Some greywacke layers (up to 20 cm thick) are also found within the diamictite. The clasts include quartzite (40–50 vol %), granite (10 vol %), sandstone (10 vol %), micaschist (4 vol %), gneiss (2 vol %), shale (1 vol %), jasper (1 vol %), siliceous dolomite (0, 5–1 vol %) and orthoclase (0.5 vol %). This diamictite with a laminated argillaceous sandy matrix is described under microscope as a lithic greywacke and was observed on samples from 227 m, 228 m and 232 m of drill hole MWAS0001. The matrix consists of mud, chlorite and carbonate. The matrix also includes mono-mineralic quartz grains, with lesser feldspars and minor chlorite after mafic phases (Fig. 5c). It is very fine-grained and commonly between 30 and 70 vol %. Rare detrital grains of muscovite and zircon are also observed. Rounded brown to greenish blue tourmaline (in plane polarised light) is a common accessory mineral and reaches sizes up to 1 mm (Fig. 5b). The lithic fragments are typically poorly sorted, angular, rounded to moderately rounded and range in size from millimetre to centimetre. They are of variable composition with clasts of felsic (Fig. 5d) or mafic orthogneisses, quartzites and schists. Other un-metamorphosed fragments include mafic volcanics, sandstone, micritic carbonate and graphite-rich clasts.

Unit 5 (U5, 160 m thick) consists of a diamictite, which includes sandstone, siltstone, shale and orthoconglomerate layers in its upper part. The clasts constituting the diamictite include quartzite (50 vol %), siliceous dolomite (10 vol %), quartz (10 vol %), granite (7 vol %), mica schist (5 vol %), sandstone (3 vol %), basalt (~1 vol %), shale (~1 vol %) and orthoclase (~1 vol %) in a chlorite-rich massive argillaceous matrix. Some angular-shaped hematite concretions are observed, replacing carbonate clasts or filling fractures.

Lenses of detrital packages are found in the diamictite showing erosional surface contacts, which suggests intermittent sedimentation. The orthoconglomerate (1–2 m thick) contains well-sorted, rounded clasts of quartzite (50–65 vol %), quartz (10–20 vol %), sandstone (5 vol %) and siliceous dolomite (3 vol %) within an iron-rich massive to laminated sandy matrix. Massive sandstones (10–20 cm thick) contain some conglomeratic and arkosic beds, and silstones (15–20 cm thick) are bedded and locally show cross bedding. Shales (10–15 cm thick) are laminated and characterised by planar to wavy bedding. Some sequences with basal orthoconglomerate overlain successively by sandstone, siltstone and shale beds are observed. Cross bedding is very common inside these sequences and the sandy beds are well sorted and show graded bedding. Post-depositional structures and soft sediment deformation structures are similar to those described in Unit 1 (Fig. 4c–f and h).

The sandstones are described as arkosic sandstones, mineralogically immature and moderately well sorted. They are characterised by the presence of cross bedding, lamination and rip-up

clasts of very fine mudstone and/or graphitic material. Grains are monocrystalline and typically tabular or angular in shape (Fig. 5e and f). Mineral grains identified in the sandstone include abundant chlorite (35 vol %) and feldspars (35 vol %), angular quartz (~10 vol %) and hematite (2 vol %). Rip-up clasts constitute the remaining ~10 vol % of the rock volume. The quartz grains are clean and some have undulose extinction under crossed polars. Chlorite grains form after mafic minerals, possibly pyroxenes and amphiboles that have undergone chloritisation at some stage. The feldspars are commonly dusty and sericitised, and both K-feldspars and plagioclases are recognised. These arkosic sandstones contain laminations on a millimetric scale of fine mud and carbonaceous material, and occasionally rip-up clasts. The fine matrix is dominated by opaque iron oxides. Detrital Fe-Ti oxides (ilmenite), hematite, detrital grains of muscovite and rutile, rare zircon and tourmaline constitute the accessory phases in the matrix. This mineralogical composition indicates that the sediment derived from a dominantly mafic source with a felsic component.

Unit 6 (U6, 52 m thick) starts with a 34 m-thick diamictite with a massive or finely laminated argillaceous matrix. The clasts are dominantly striated and consist of quartzite (88 vol %) and sandstone (10 vol %) with rare feldspar and quartz clasts. This diamictite is overlain successively by massive mudstone (8 m thick) and massive to bedded conglomeratic siltstone (10 m thick) that includes greywacke (up to 2 m thick) and bedded mudstone (2–3 m thick). Rare rounded clasts of shale and quartzite up to 1 cm in diameter and a chlorite-rich matrix constitute the conglomeratic siltstone. Some dropstones are also recognised in the massive mudstones. Quartz-hematite veins (1–1.5 cm thick) are common in this unit. Iron oxides and chlorite are very common in fractures and along the bedding.

Unit 7 (U7) was not intercepted by the drill hole MWAS0001 but was mapped on outcrops. The contact between U7 and U6 is characterised by an erosional surface. Unit 7 is a diamictite with poorly-sorted clasts in a chlorite-rich massive sandy matrix. The clasts include quartzite (60 vol %), micaschist (9 vol %), massive dolomite (8 vol %), quartz (7 vol %), bedded siliceous dolomite (5 vol %) and granite (5 vol %). Quartz-chlorite, quartz-hematite and quartz-hematite-chlorite veins crosscut both the matrix and clasts. Some larger clasts (up to 30 cm) are present at the base of U7, and some of them are striated.

## 5. Metallic mineralisation

Metallic mineralisation is found as disseminated sulphide grains in diamictite units with sandy and greywacke matrices (U2 and U3), in lithic greywacke (U4), and in orthoconglomerate, arkosic sandstone and siltstone (U5). Vein-hosted Cu mineralisation is found mostly in diamictite with a mud matrix and in mudstone (U1 to U5). The Units 6 and 7 do not have Cu mineralisation but some framboidal pyrites are disseminated in conglomeratic siltstone within these units. In general, there is a clear association between chlorite and mineralisation.

### 5.1. Mineralisation in U1, U2 and U3

The sandstones of U1 do not have disseminated sulphides (pyrite or Cu sulphide). The main Cu mineral is chalcopyrite and is restricted to the carbonate veins. Quartz veins with less carbonate or hydrothermal feldspar (adularia) are not mineralised. Authigenic chlorite-rich matrix that characterise the U2 diamictite contains disseminated pyrite, chalcopyrite and chalcocite.

The diamictite from U3 with a greywacke matrix is locally fractured and brecciated. Dolomite with minor fine-grained bornite, chalcopyrite, chlorite and hematite fill the fractures. Pyrite and chalcopyrite crystals are found disseminated only in the greywacke beds and in the interbedded layers of the diamictite characterised by a sandy matrix. Some horizons within this diamictite contain framboidal and fine euhedral pyrite crystals. These sulphides are associated with chlorite, especially in the fractures which affected both the matrix and clasts. Some sulphides are also found rimming the clasts of granite, micaschist, sandstone, quartzite and quartz. Two types of carbonate veins are distinguished, one is brownish to yellowish and contains pyrite, chalcopyrite and bornite and the other type is white and without sulphides. The second type is posterior to the precipitation of

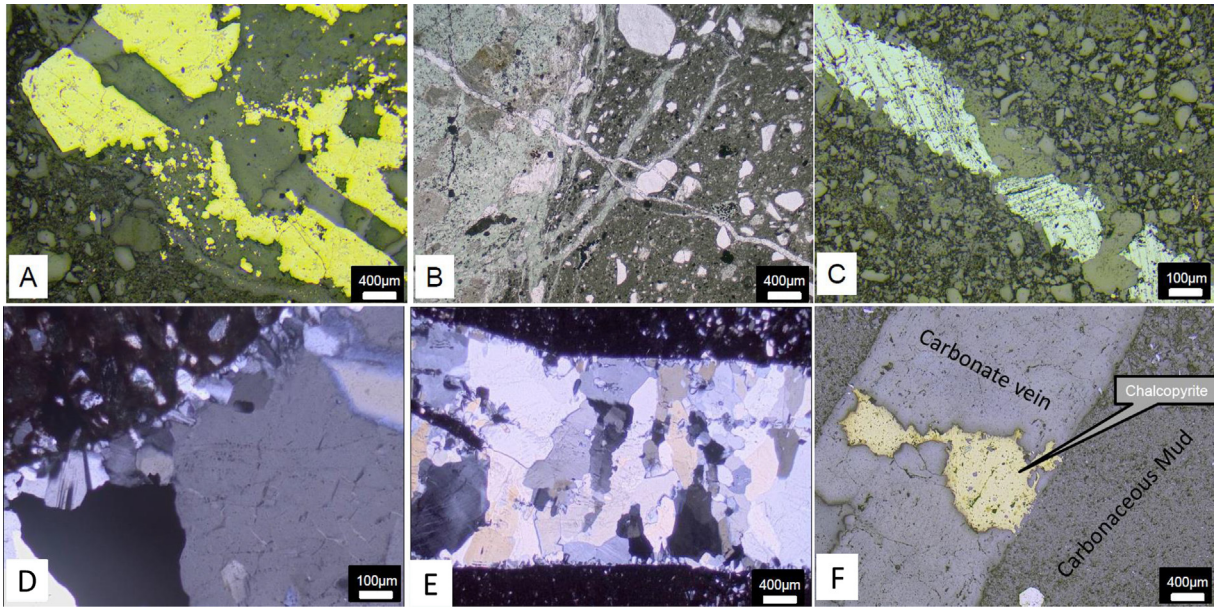


**Fig. 6.** Mineralisation types: (A) Pyrite mineralisation within a graphitic clast, and a vein with pyrite cutting this graphitic clast, (B) Gabbroic clast with numerous chlorite veins, note the late carbonate vein, (C) Bladed hematite within a carbonate quartz rich vein, (D) Top left corner of photo represents the host rock, note feldspar growth along the vein selvedge. Twinning can be seen in the feldspars, (E) Vein selvedge of feldspar followed by a later quartz infill, (F) Chalcopyrite and dolomite vein (reflected image).

sulphide mineralisation.

### 5.2. Mineralisation in U4

The lithic greywacke contains very fine-grained disseminated pyrite throughout the matrix. Some mafic clasts commonly include pyrite that increases in concentration and grain size towards the core of the clast. Quartz-carbonate veins are rich in pyrite in places where they crosscut graphitic or carbonaceous layers. Fig. 6a shows abundant pyrite in a quartz-carbonate vein that crosscuts a fine-grained carbonaceous clast.

Three generations of veins are observed and their width varies from millimetre to centimetre. The two oldest generations are not observed to crosscut each other so their timing relationship is unknown, but they are compositionally different. The first vein generation is constituted by quartz with traces of carbonate (dolomite?). The larger veins commonly have feldspar (adularia) as the first phase to precipitate on the selvedges. Quartz is often a minor component commonly associated with adularia, but in variable amount. Fine-grained filamentous, mm-wide veins are sometimes dominated by adularia and quartz. Adularia, carbonate and quartz veins have a core filled with bladed hematite up to 2 mm wide, suggesting the oxidation of the fluid (Fig. 6c). The second generation is characterised by a fine network of chlorite-carbonate veins (Fig. 6b). The third generation is a carbonate-chlorite vein containing Cu sulphides and cuts the two early vein generations.

### 5.3. Mineralisation in the U5

Euhedral and framboidal pyrite, chalcopyrite and bornite are found disseminated in the sandy matrix of orthoconglomerate, arkosic sandstone and siltstone beds. However, more sulphides are found where authigenic chlorite is abundant. Locally, fine bornite and chalcopyrite crystals are found disseminated in chlorite-rich sandstone.

In the fluvial facies of Unit 5, millimetric veins comprise fine-grained (0.25 mm) feldspar (adularia) nucleating as vein-selvedge and growing inwards, occasionally with quartz (Fig. 6d and e). Other veins include coarse-grained quartz, carbonate (calcite), chalcopyrite and later pyrite. Chalcopyrite is restricted to where the vein intersects carbonaceous mud layers, which represent a reduced environment and contain locally abundant framboidal pyrite. This local environment recognised in some horizons is favoured to precipitate copper from the fluids through the oxydo-reduction reaction.

In the diamictite, euhedral pyrite crystals are the dominant sulphides compared to chalcopyrite. Framboidal pyrite is usually found replaced by chalcopyrite or with chalcopyrite overgrowth. Pyrite and chalcopyrite are also found on the rims of clasts, along the fractures and always associated with chlorite. The diamictite contains a lot of small clasts (<1 cm) rich in chlorite with a lot of pyrite and chalcopyrite. There are also some dolomite veins containing pyrite, chalcopyrite, hematite and minor chlorite.

## 6. Discussion

### 6.1. Depositional model

The Mwale Formation within the Katangan basin hosts several depositional facies including continental, glaciogenic and glaciomarine sediments (Binda and Van Eden, 1972; Master and Wendorff, 2011). The lithological succession defined at Shanika syncline (Fig. 3) contrasts with the succession observed at the Kamoa Cu deposit where only siltstone and greywacke are interbedded within the diamictite (Schmandt, 2012; Schmandt et al., 2013). Although the upper part of the diamictite do not occur at Shanika syncline, the Mwale Formation shows at least seven glacial sequences, corresponding to the seven units described above. Each glacial episode was succeeded by marine, fluvial or lacustrine episodes. The contact between the glaciofluvial and glaciomarine units with the glaciogenic units is marked by an erosional surface (e.g., U1, U2 and U5). This suggests that the deposition of the diamictite layer was followed by an alternation of quiet and turbulent periods in the basin.

The lithological succession of the Mwale Formation at Shanika syncline shows a vertical variation over time. Glaciogenic sediments are hosted within glaciomarine sediments, suggesting a proglacial marine facies zone. It is followed by a succession of glaciogenic beds within glaciofluvial and glaciolacustrine facies, which we interpret as indication of a proglacial zone in terrestrial landforms. These two distinct paleoenvironments indicate that the glacial conditions alternated during two episodes of advancing and retreating ice sheets, (as discussed by Reading, 1996). Similar observations have been described in the Upper Smalfjord Formation of the Upper Proterozoic at north Norway (Edwards, 1984).

#### 6.1.1. Evidence for a marine setting

Some successions identified in U1 and U2 are typical of a Bouma sequence, consisting of orthoconglomerate overlain by arkosic sandstone, siltstone and massive and laminated mudstone. Slump structures are also observed in these sequences. This Bouma sequence is a characteristic of turbidites within debris flow deposits in a marine environment (Eyles, 1990). The debris flow deposits are also common in the upper diamictite of the West Congolian (Delpomdor et al., 2016). In the case of the Mwale Formation, the debris flow deposition was normally induced by basin-wide tectonic movement (Buffard, 1988; Kampunzu et al., 1993) and glacial influence. The neptunian dykes with sand filling cracks in the mudstone, and sill injections characterised by the injection of mudstone in sandstone beds, groove and roll marks in mudstone beds and erosional surfaces observed in the U1 and U2 are indicative of a deep water marine environment. These observations suggest that the Mwale Formation includes several marine conditions and cannot be considered as deposited during a single glaciomarine event (e.g., U1 and U2). The deposition of marine beds within a diamictite is also mentioned in other Neoproterozoic diamictites (Ali et al., 2010; Eyles and Januszczak, 2004).

#### 6.1.2. Evidence for fluvial and lacustrine settings

Glaciofluvial sedimentation in a shallow water delta environment of the Mwale Formation is indicated by the presence of high-angle cross bedding, rip-up clasts, the immaturity of the sandstone, poor to moderate sorting of the clasts and the presence of some angular clasts suggesting proximity to the source and rapid sedimentation. Rhythmic sequences hosting arkosic sandstone and siltstones with both massive and laminated mudstones are observed. These mudstone beds are host to groove, roll and flute marks, as well as load deformation structures such as some primary inorganic sedimentary structures (Selley, 2000). These structures are not only typical of a glaciomarine environment (e.g. U1 and U2); they are also associated with glaciofluvial deposits at Shanika syncline (e.g. U5). Soft sediment deformations in conglomerate and sandstone of the glacial Smalfjord Formation (Northern Norway) were also interpreted as indicative of glaciofluvial deposition (Arnaud, 2008).

These primary inorganic sedimentary structures were also described in other Palaeoproterozoic and Neoproterozoic glacial deposits, e.g., Port Askaig Tillite in Scotland (Panahi and Young, 1997), Gowganda Formation in Canada (Young and Nesbitt, 1999), Mineral Fork Formation in Utah (Young, 2002), and the Witvlei

Group in Namibia (Gorjan et al., 2003). The Mineral Fork Formation includes some mudrock layers within the diamictite, and locally some turbidite features including graded bedding, flute and load casts, and fine lamination. The upper set of mudstone and conglomeratic siltstone in Unit 6 indicates a glaciolacustrine environment. This is supported by the presence of dropstones in massive mudstone as discussed by Reading (1996), also found in the Late Proterozoic Adrar of Mauritania (Deynoux, 1985), and by the rhythmites with dispersed clasts observed in the conglomeratic siltstone.

#### 6.1.3. Origin of the clasts

The clasts constituting the Mwale Formation in the Shanika syncline include metamorphic and magmatic rocks (quartzite, micaschist, granite, gneiss, orthoclase and quartz), and sedimentary rocks (siliceous dolomite, oolitic dolomite, shale, sandstone and jasper). Quartzite clasts are the most abundant (up to 85 vol %). Some of these clasts are faceted or striated. Available geochronological data from detrital zircons and muscovite suggest that most of the pre-Katangan rocks surrounding the Katangan basin supplied the sediments (Batumike et al., 2007b; Master et al., 2005). However, considering the location of Shanika syncline, the Kibara belt, located to the north of the belt, is the best candidate for the quartzite, micaschist, gneiss, granite, orthoclase and quartz clasts. The sedimentary rock clasts may be of intrabasinal origin, deriving from the underlying Mwashya Subgroup and part of the Kansuki Formation in which these typical lithologies are observed (Cailteux et al., 2007), and that are missing in the Shanika area. Similar erosion of the Mwashya-Kansuki succession has been observed in the Fungurume-Kolwezi area (Cailteux, 1991, 1994; Cailteux et al., 2007; François, 1973).

### 6.2. Hydrothermal alteration

Vein-type Cu-Pb-Zn mineralisation in the Nguba Group along the Congo Copperbelt was documented at Kipushi, Lombe and Kengere (Chabu and Boulègue, 1992; De Magnée and François, 1988; Intiomale and Oosterbosch, 1974; Kamona et al., 1999; Kampunzu et al., 2009). These mineralisations are hosted in the carbonates of Kaponda, Kakontwe and Kipushi formations and in the shales and carbonates of the Katete Formation (Kampunzu et al., 2009). However, at Kamoa, Tombolo, Fisthie and Shanika, the mineralisation is hosted in the Mwale Formation that is stratigraphically beneath the Kaponda and Kakontwe formations (Batumike et al., 2007a). Cu mineralisation within the Mwale Formation exhibits different features within the Congo-Zambia Copperbelt. At Kamoa, Cu mineralisation is associated with minor Zn (sphalerite) (Schmandt et al., 2013) whereas it is associated with iron oxide (magnetite) at Fishtie (Hendrickson et al., 2015). At Shanika, Cu mineralisation is low grade and not associated with other metals; however, hematite was locally observed in mineralised veins, mostly toward the top of the succession.

The style of the mineralisation at Shanika syncline shows some particular features. Euhedral and framboidal pyrites found in the Mwale Formation at the Shanika may have a diagenetic origin. Although they occur in the chlorite-rich matrix, they are also observed where chlorite is absent. Diagenetic pyrites are known all over the Congo-Zambia Copperbelt (Cailteux et al., 2005; De Waele et al., 2006; El Desouky et al., 2009, 2010; Haest and Muchez, 2011; Hitzman et al., 2012; Muchez et al., 2015; Schuh et al., 2012; Schmandt, 2012). The precipitation of Cu minerals in dolomite-chlorite veins, where these veins crosscut reduced horizons suggest that the mineralising fluid was Mg-rich and the disseminated Cu mineralisation could also be the result of the same mineralising fluid in the porous rock.

Two main episodes of sulphide ore mineral precipitation are found in the Mwale Formation at the Shanika syncline. The first consists of diagenetic pyrite in the diamictite. The second is the hydrothermal event recognised in the glagiocenic, glaciomarine and glaciofluvial horizons, which indicates a possible vertical zonation and lithological control (Table 2). This second generation consists of dissemination of chalcopyrite, bornite and chalcocite in the matrix of lithic greywacke, orthoconglomerate, arkosic sandstone and siltstone and the precipitation of Cu sulphides with pyrite in carbonate-chlorite or carbonate-quartz-chlorite veins and in fractures. These mineralised fractures crosscut both clasts and matrix. In places, there is a replacement of earlier pyrite by chalcopyrite or chalcopyrite rims around clasts. The vertical distribution, structural and lithological controls of Cu sulphide defined at Shanika syncline are not similar to observations at the Kamoa and Fishtie deposits (Table 2). At Fishtie deposit, high-angle normal faults bear Cu mineralisation and a horizontal zonation is developed around each fault (Hendrickson et al., 2015). In contrast at Kamoa, sulphides show a vertical zonation without structural control. This zonation is recognised from the contact of the footwall sandstone upwards through the lower diamictite to the lower pyritic siltstone with chalcocite, bornite, chalcopyrite and pyrite zones (Schmandt et al., 2013). This suggests different styles of mineralisation occur within the Mwale Formation in different geographical locations inside the Katanga basin. The common aspect between the observations at Shanika syncline and Kamoa is the presence of sulphide rimming clasts, which is also observed in other locations within the copperbelt.

Fay and Barton (2012) and Schuh et al. (2012) identified three types of hydrothermal metasomatism in the Mines Subgroup (Table 1) at TFMD: magnesian, sodic and potassic alterations. Oosterbosch (1950) and Schuh et al. (2012) highlighted a close relationship between Cu-Co sulphides and Mg-chlorite in the 'Roches Silliceuses Feuilletées' (RSF, Table 1) and 'Dolomie Stratifiée' (D.Strat, Table 1) at Kwatebala (close to the Shanika syncline, Fig. 2) and the Fungurume Cu-Co deposit. The Mwale Formation at Shanika syncline also indicates a relationship between Cu sulphides and magnesian hydrothermal alteration, i.e., the presence of chlorite. Cu sulphides including chalcopyrite and bornite are abundant in chlorite-rich layers. Muchez et al. (2008) also demonstrated the presence of hypogene Cu mineralisation related to Mg-metasomatism (chlorite) in the Congo Copperbelt. Potassic alteration indicated by K-feldspar (adularia) as vein selvedge and silicification with quartz vein have also affected the Mwale Formation; however, no clear relationship is observed between potassic alteration or silicification and Cu mineralisation at the Shanika syncline. Contrastingly, Hitzman et al. (2012) indicated widespread potassic alteration related to mineralisation in the Zambia Copperbelt. Schmandt et al. (2013) indicated that potassic alteration and silicification are also the main hydrothermal alteration stages controlling the precipitation of Cu mineralisation at Kamoa while the magnesian hydrothermal alteration post-dates most sulphide precipitation (e.g., chalcopyrite, chalcocite, bornite and sphalerite). The Kamoa deposit is lithologically similar to the siliciclastic-hosted deposits of the Zambia Copperbelt (Hitzman et al., 2012; Schmandt et al., 2013; Selley et al., 2005).

The magnesian metasomatism (chlorite) is late to post-orogenic in the Congo Copperbelt. It should therefore correspond to one of the extensional brittle tectonic stages (stage 4 or 5) of Kipata et al. (2013). The fact that carbonate-chlorite-Cu sulphide veins crosscut unmineralised carbonate-feldspar-quartz veins and feldspar-quartz veins suggests that chloritisation was a late event. Hematite veins are the result of a later oxididation, posterior to the deposition of metals (Cailteux et al., 2005; Muchez et al., 2010). Similar vein-type Cu mineralisation is known in the Mines Subgroup and was

interpreted as related to a late hydrothermal and metasomatic event affecting the copperbelt as observed at Kwatebala and Fungurume Cu-Co deposits in the DRC and at the Fishtie Cu deposit in Zambia (Hendrickson et al., 2015; Schuh et al., 2012).

## 7. Conclusion

Seven different lithological sequences (U1 to U7) are distinguished within the Mwale Formation at Shanika syncline. Each of these units contains a basal diamictite overlain by orthoconglomerate, sandstone, siltstone, shale and mudstone layers. This indicates that the Mwale Formation was deposited during several (at least seven) sedimentary episodes which are characterised by glaciogenic with glaciomarine sedimentation in the proglacial marine facies zone and glaciogenic with glaciofluvial and glaciolacustrine sedimentation in a terrestrial proglacial zone. Evidence of debris flow induced by glaciation in the marine environment is indicative of glaciomarine deposition (U1 and U2). The presence of high-angle cross bedding, rhythmic deposition of siltstone and mudstone or arkosic sandstone and siltstone in Unit 5 are characteristic of a glaciofluvial environment. Occurrence of dropstones in laminated mudstone beds and rhythmites with dispersed clasts observed in the conglomeratic siltstone characterise a glaciolacustrine environment.

The clasts in the diamictite beds are dominantly composed of quartzite, and quartz, shale, sandstone, granite, dolomite, gneiss and mafic rocks. Some of the clasts are faceted and striated with varying size (mm to 80 cm of diameter). The matrix is mainly constituted of angular to subangular clasts, indicating a short distance of transportation, and contrasting with rounded clasts (i.e. long distance of transportation) present in the diamictite. This suggests an immature nature of the matrix and a different provenance of the clasts.

The mineralising fluid was Mg-rich as indicated by the presence of abundant chlorite. The oxidised mineralising fluid reacted with the reduced horizons to precipitate copper, getting the required sulphur from these reduced layers that contain abundant framboidal pyrite. The mineralised veins are associated with magnesian alteration as indicated by abundant chlorite, and are younger than feldspar and quartz veins that are characteristic of potassic alteration and silicification. The same mineralising fluid could also have affected the porous horizons of the Mwale Formation as seen by the presence of disseminated mineralisation. This Mg-metasomatism is a late hydrothermal event compared to potassic alteration (adularia) and silicification. This is similar to the magnesian hydrothermal activity identified in the Mines Subgroup (at Fungurume deposit) and Mwale Formation (at Kamoa and Fishtie deposits).

## Acknowledgements

This paper is a contribution to the ore genesis of the Cu-(Pb, Zn) mineralisation in both the Kundelungu and Nguba Groups along the Lufilian arc currently ongoing at the University of Lubumbashi (Department of Geology) and the KU Leuven (Geodynamics and Geofluids Research Group, Department of Earth and Environmental Sciences). Freeport Mc-MoRan is thanked for authorising the publication of the results. Robert North, Isabelle Fay, Joseph Nzita and Theophilus Osei-Poku are also thanked for documentation. Alain Mukanzila, Bejamin Kivunge, Dieudonné Musuil, Fiston Kabo, and Floris Kasongo of Tenke Fungurume Mining are thanked for their support during fieldwork and core logging. This research was funded by the Belgian Development Cooperation under project RA_S1_RDC_GEODYN-SUIVI to D. Delvaux. This is contribution 934 from the ARC Centre of Excellence for Core to Crust Fluid Systems (http://www.ccfs.mq.edu.au) and 1141 from the GEMOC Key Centre (http://www.gemoc.mq.edu.au). The journal chief editor (R. Mapeo), J. Cailteux and F. Delpomdor are thanked for their remarks and corrections that allowed improving the quality of the paper.

## References

Ali, K.A., Stern, R.J., Manton, W.I., Johnson, P.R., Mukherjee, S.K., 2010. Neoproterozoic diamictite in the eastern desert of Egypt and northern Saudi Arabia: evidence of ~750 Ma glaciation in the arabian-nubian shield? Int. J. Earth Sci. 99, 705–726.

Armstrong, R.A., Master, S., Robb, L.J., 2005. Geochronology of the nchanga granite, and constraints on the maximum age of the Katanga supergroup, zambian copperbelt. J. Afr. Earth Sci. 42, 32–40.

Arnaud, E., 2008. Deformation in the Neoproterozoic Smalfjord Formation, northern Norway: an indicator of glacial depositional conditions? Sedimentology 55, 335–356.

Batumike, J.M., Belousova, E., Griffin, W.L., Lubala, R.T.F., Chabu, M., Kaseti, K.P., Djuma, B.A., Ferriere, L., 2016. Perovskite U-Pb age of the Katuba kimberlite, Kundelungu Plateau (D.R. Congo): implications for regional tectonism and mineralisation. South Afr. J. Geol. submitted for publication.

Batumike, J.M., Kampunzu, A.B., Cailteux, J.H., 2006. Petrology and geochemistry of the neoproterozoic and Nguba Kundelungu groups, Katanga supergroup, southeast Congo: implication for provenance and geotectonic setting paleoweathering. J. Afr. Earth Sci. 44, 97–115.

Batumike, M.J., Kampunzu, A.B., Cailteux, J.H., 2007a. Lithostratigraphy, basin development, base metal deposits, and regional correlations of the Neoproterozoic Nguba and Kundelungu rock successions. Central Afr. Copperbelt. Gondwana Res. 11, 432–447.

Batumike, J.M., O'Reilly, S.Y., Griffin, W.L., Belousova, E.A., 2007b. U-Pb and Hf isotope analyses of zircon from the Kundelungu Kimberlites, D.R.Congo: implication for crustal evolution. Precambrian Res. 156, 195–225.

Berkman, D.A., 2001. Field Geologists' Manual, fourth ed. Australian Institute of Mining and Metallurgy, Carlton, p. 395.

Binda, P.L., Van Eden, J.G., 1972. Sedimentological evidence for the origin of the precambrian great conglomerate (Kundelungu tillite), Zambia. Palaeogeogr. Palaeoclimatol. Palaeoecol. 12, 151–168.

Boyle, R.A., Lenton, T.M., Williams, H.T.P., 2007. Neoproterozoic 'snowball Earth' glaciations and the evolution of altruism. Geobiology 5, 337–349.

Broughton, D., Rogers, T., 2010. Discovery of the Kamoa copper deposit, central Africa copperbelt, D.R.C. Soc. Econ. Geol. Special Publ. 15 (1), 287–298.

Buffard, R., 1988. Un rift intracontinental du Précambrien supérieur: Le Shaba méridional (Zaïre). Doctorate Thesis. University of Maine, France, p. 316.

Cailteux, J., 1991. La tectonique intra-katanguienne dans la région Nord-ouest de l'arc Lufilien (Shaba, Rép. du Zaïre). Ann. la Société Géologique Belg. 113, 199–2015.

Cailteux, J., 1994. Lithostratigraphy of the neoproterozoic shaba-type (zaïre) roan supergroup and metallogenesis of associated stratiform mineralisation. In: Kampunzu, A.B., Lubala, R.T. (Eds.), Neoproterozoic Belts of Zambia, Zaïre and Namibia. Journal of African Earth Sciences, vol. 19, pp. 279–301.

Cailteux, J., Binda, P.L., Katekesha, W.M., Kampunzu, A.B., Intiomale, M.M., Kapenda, D., Kaunda, C., Ngongo, K., Tshiauka, T., Wendorff, M., 1994. Lithostratigraphical correlation of the neoproterozoic roan supergroup from shaba (zaïre) and Zambia in the central african copper-cobalt metallogenic province. In: Kampunzu, A.B., Lubala, R.T. (Eds.), Neoproterozoic Belts of Zambia, Zaïre and Namibia. Journal of African Earth Sciences, vol. 19, pp. 265–278.

Cailteux, J.L.H., Kampunzu, A.B., Lerouge, C., 2007. The Neoproterozoic Mwashya-Kansuki sedimentary rock succession in the central African Copperbelt, its Cu-Co mineralisation, and regional correlations. Gondwana Res. 11, 414–431.

Cailteux, J.L.H., Kampunzu, A.B., Lerouge, C., Kaputo, A.K., Milesi, J.P., 2005. Genesis of sediment-hosted stratiform copper-cobalt deposits, Central African Copperbelt. J. Afr. Earth Sci. 42, 134–158.

Chabu, M., Boulègue, J., 1992. Barian feldspar and muscovite from the Kipushi Zn-Pb-Cu deposit, shaba zaïre. Can. Mineral. 30, 1143–1152.

De Magnée, I., François, A., 1988. The origin of the Kipushi (Cu, Zn, Pb) deposits in direct relation with a proterozoic salt diapir. Copperbelt of central Africa, shaba, republic of zaïre. In: Friedrich, G.H., Herzig, P.M. (Eds.), Base Metal Sulfide Deposits. Berlin Heidelberg. Springer-Verlag, pp. 74–93.

De Putter, T., Mees, F., Decrée, S., De Waele, S., 2010. Malachite, an indicator of major pliocene Cu remobilization in a karstic environment (Katanga, democratic republic of Congo). Ore Geol. Rev. 38, 90–100.

De Waele, S., Muchez, Ph, Vets, J., Fernandez-Alonzo, M., Tack, L., 2006. Multiphase origin of the Cu-Co deposits in the western portion of the Lufilian fold-and-thrust belt, Katanga (Democratic Republic of Congo). J. Afr. Earth Sci. 46, 455–469.

Delpomdor, F., Eyles, N., Tack, L., Préat, A., 2016. Pre- and post-Marinoan carbonate facies of the Democratic Republic of the Congo: glacially- or tectonically-influenced deep-water sediments? Palaeogeogr. Palaeoclimatol. Palaeoecol. 457, 144–157.

Deynoux, M., 1985. Terrestrial or waterlain glacial diamictites? Three case studies from the Late Precambrian and Late Ordovician glacial drifts in West Africa. Paleogeogr. Paleoclimatol., Paleoecol. 51, 97–141.

Edwards, M.B., 1984. Sedimentology of the upper proterozoic glacial record,

vestertana group, finnmark, north Norway. Norges geologiske undersøkelse. Bulletin 394, 76.
El Desouky, H.A., Muchez, Ph, Boutwood, A., Tyler, R., 2008. Postorogenic origin of the stratiform Cu mineralisation at lufukwe, lufilian foreland, democratic republic of Congo. Econ. Geol. 103, 555–582.
El Desouky, H.A., Muchez, Ph, Boyce, A.J., Schneider, J., Cailteux, J.L.H., De Waele, S., Von Quadt, A., 2010. Genesis of sediment-hosted stratiform copper-cobalt mineralisation at luiswishi and kamoto, Katanga copperbelt (democratic republic of Congo). Miner. Deposita 45, 735–763.
El Desouky, H.A., Muchez, Ph, Cailteux, J., 2009. Two Cu-Co sulfide phases and contrasting fluid systems in the Katanga Copperbelt, Democratic Republic of Congo. Ore Geol. Rev. 36, 315–332.
Eyles, N., 1990. Marine debris flows: late Precambrian tillites of the Avalonian-Cadomian orogenic belt. Palaeogeogr. Palaeoclimatol. Palaeoecol. 79, 73–98.
Eyles, N., Januszczak, N., 2004. "Zipper-rift": a tectonic model for Neoproterozoic glaciations during the breakup of Rodinia after 750 Ma. Earth Sci. Rev. 65, 1–73.
Fay, I., Barton, M., 2012. Alteration and ore distribution in the proterozoic Mines series, tenke-fungurume Cu–Co district, democratic republic of Congo. Miner. Deposita 47, 501–519.
François, A., 1973. L'extrémité occidentale de l'arc cuprifère Shabien. Etude géologique. Mémoire du département géologique, Gécamines, Likasi (République du Zaïre), p. 65.
François, A., 1987. Synthèse géologique sur l'arc cuprifère du Shaba (Rép. du Zaïre). Centenaire de la Société Belge de Géologie, pp. 15–65.
François, A., 2006. La partie centrale de l'Arc cuprifère du Katanga. Tervuren (Belgique). Afr. Geosci. Collect. 109, 70.
Goddéris, Y., Donnadieu, Y., Nédélec, A., Dupré, B., Dessert, C., Grard, A., Ramstein, G., François, L.M., 2003. The Sturtian 'snowball' glaciation: fire and ice. Earth Planet. Sci. Lett. 211, 1–12.
Gorjan, P., Walter, M.R., Swart, R., 2003. Global Neoproterozoic (Sturtian) post-glacial sulfide–sulfur isotope anomaly recognised in Namibia. J. Afr. Earth Sci. 36, 89–98.
Graham, A.S., Susannah Porter, S., Halverson, G.P., 2016. A new rock-based definition for the Cryogenian Period (circa 720–635 Ma). Episodes J. Int. Geosci. 39, 1–8.
Haest, M., Muchez, Ph, 2011. Stratiform and vein-type deposits in the Pan-African orogen in central and southern Africa: evidence for multiphase mineralisation. Geol. Belg. 14, 23–44.
Hanson, R.E., Wardlaw, M.S., Wilson, T.J., Mwale, G., 1993. U-Pb zircon ages from the Hook granite massif and Mwembeshi dislocation: constraints on Pan-African deformation, plutonism, and transcurrent shearing in central Zambia. Precambrian Res. 63, 189–209.
Hendrickson, M.D., Hitzman, M.W., Wood, D., Humphrey, John D., Wendlandt, R.F., 2015. Geology of the Fishtie deposit, Central Province, Zambia: iron oxide and copper mineralisation in Nguba Group metasedimentary rocks. Miner. Deposita 50, 717–737.
Hitzman, M.W., Broughton, D., Selley, D., Woodhead, J., Wood, D., Bull, S., 2012. The Central African Copperbelt: diverse stratigraphic, structural and temporal settings in the world's largest sedimentary copper district. Soc. Econ. Geol. Special Publ. 16, 487–514.
Hoffman, P.F., Kaufman, A.J., Halverson, G.P., Schrag, D.P., 1998. A neoproterozoic snowball earth. Science 281, 1342–1346.
Hoffman, P.F., Schrag, D.P., 2002. The snowball Earth hypothesis: testing the limits of global change. Terra Nova. 14, 129–155.
Intiomale, M.M., Oosterbosch, R., 1974. Géologie et géochimie du gisement de Kkipushi, Zaïre. In: Bartholomé, P. (Ed.), Gisements Stratiformes et Provinces Cuprifères. Centenaire de la Société Géologique de Belgique, Liège, pp. 123–164.
Jackson, M.P.A., Warin, O.N., Woad, G.M., Hudec, M.R., 2003. Neoproterozoic allochthonous salt tectonics during the Lufilian orogeny in the Katangan Copperbelt, central Africa. Geol. Soc. Am. Bull. 115, 314–330.
Kamona, A.F., Lévêque, J., Friedrich, G., Haack, U., 1999. Lead isotopes of the carbonate-hosted kabwe, tsumeb, and Kipushi Pb-Zn-Cu sulphide deposits in relation to Pan african orogenesis in the damaran-lufilian fold belt of central Africa. Miner. Deposita 34, 273–283.
Kampunzu, A.B., Cailteux, J., 1999. Tectonic evolution of the Lufilian arc (central african copperbelt) during neoproterozoic Pan-African orogenesis. Gondwana Res. 2, 401–421.
Kampunzu, A.B., Cailteux, J.H., Kamona, A.F., Intiomale, M.M., Melcher, F., 2009. Sediment-hosted Zn-Pb-Cu deposit in the central african copperbelt. Ore Geol. Rev. 35, 263–297.
Kampunzu, A.B., Kanika, M., Kapenda, D., Tshimanga, K., 1993. Geochemistry and geotectonic evolution of late Proterozoic Katangan basic rocks from the Kibambale in central Shaba (Congo). Geol. Rundsch. 82, 619–630.
Kampunzu, A.B., Tembo, F., Matheis, G., Kapenda, D., Huntsman-Mapila, P., 2000. Geochemistry and tectonic setting of mafic igneous units in the Neoproterozoic Katanga Basin, Central Africa: implications for Rodinia break-up. Gondwana Res. 3, 125–153.
Key, R.M., Liyungu, A.K., Njamu, F.M., Somwe, V., Banda, J., Mosley, P.N., Armstrong, R.A., 2001. The western arm of the Lufilian Arc in NW Zambia and its potential for copper mineralisation. Afr. Earth Sci. 33, 503–528.
Kipata, M.L., Delvaux, D., Sebagenzi, M.N., Cailteux, J., Sintubin, M., 2013. Brittle and stress field evolution in the Pan-African Lufilian and its foreland (Katanga, DRC): from orogenic compression to extensional collapse, transpressional inversion and transition to rifting. Geol. Belg. 16, 1–17.
Le Heron, D., Busfield, M., Kamona, F., 2013. An interglacial on snowball Earth? Dynamic ice behaviour revealed in the Chuos Formation, Namibia. Sedimentology 60 (2), 411–427.
Master, S., Rainaud, C., Armstrong, R.A., Phillips, D., Robb, L.J., 2005. Provenance ages of the neoproterozoic Katanga super group (african central, copperbelt) with implication for basin evolution. Megabreccia from mufulira, copperbelt of Zambia. J. Afr. Earth Sci. 42, 61–81.
Master, S., Wendorff, M., 2011. Neoproterozoic glaciogenic diamictites of the Katanga supergroup, central Africa. In: Arnaud, E., Halverson, G.P., Shield-Zhou, G. (Eds.), The Geological Record of Neoproterozoïc Neoproterozoic Glaciation, vol. 36. Geological Society of London, Memoirs, pp. 173–184.
Meert, J.G., Van der Voo, R., 1997. The assembly of gondwana 800-550 Ma. J. Geodyn. 23, 223–235.
Muchez, Ph, André-Mayer, A.S., El Desouky, A.H., Reisberg, L., 2015. Diagenetic origin of the stratiform Cu–Co deposit at kamoto in the central african copperbelt. Miner. Deposita 50, 437–447.
Muchez, Ph, Brems, D., Clara, E., De Cleyn, A., Lammens, L., Boyce, A., De Muynck, D., Mukumba, W., Sikazwe, O., 2010. Evolution of Cu-Co mineralizing fluids at nkana mine, central african copperbelt, Zambia. J. Afr. Earth Sci. 58, 457–474.
Muchez, Ph, Vanderhaeghen, P., El Desouky, H., Schneider, J., Boyce, A., De Waele, S., Cailteux, J., 2008. Anhydrite pseudomorphs and origin of stratiform Cu-Co ores in the Katanga copperbelt (democratic republic of Congo). Miner. Deposita 43, 575–589.
Oosterbosch, R., 1950. La Série des Mines dans le Polygone de Fungurume. Comité Spécial du Katanga (CSK), Comptes rendus des travaux du Congrès Scientifique. Elisabethville 14, 1–18.
Oosterbosch, R., 1962. Les minéralisations dans le système de Roan au Katanga. In: Lombard, J., Nicolini, P. (Eds.), Gisements Stratiformes de Cuivre en Afrique, 1ère Partie, pp. 71–136. Copenhagen.
Panahi, A., Young, G.M., 1997. A geochemical investigation into the provenance of the neoproterozoic Port Askaig tillite, dalradian supergroup, western Scotland. Precambrian Res. 85, 81–96.
Reading, H.G., 1996. Sedimentary Environments: Processes, Facies and Stratigraphy, 3ed edition. Blackewell Publishing, p. 688.
Schmandt, D., 2012. Stratigraphy and Mineralisation of the Kamoa Cu Deposit, Katanga, Democratic Republic of Congo. Unpublished M.S. thesis, Golden, Colorado, Colorado School of Mines, p. 89.
Schmandt, D., Broughton, D., Hitzman, M.W., Plink-Bjorklund, P., Edwards, D., Humphrey, J., 2013. The Kamoa copper deposit, democratic republic of Congo: stratigraphy, diagenetic and hydrothermal alteration, and mineralisation. Econ. Geol. 108, 1301–1324.
Schuh, W., Leveille, R.A., Fay, I., North, R., 2012. Geology of the tenke-fungurume sediment-hosted strata-bound copper-cobalt district, Katanga, democratic republic of Congo. Soc. Econ. Geol. Special Publ. 16, 269–301.
Selley, D., Broughton, D., Scott, R., Hitzman, M., Bull, S., Large, R., McGoldrick, P., Croaker, M., Pollington, N., Barra, F., 2005. A new look at the geology of the Zambian Copperbelt. In: Economic Geology 100th Anniversary Volume, pp. 965–1000.
Selley, R.C., 2000. Applied Sedimentology, second ed. Academic Press, p. 446.
Shanmugam, G., 1997. The Bouma Sequence and the turbidite mind set. Earth-Sci. Rev. 42, 201–229.
Taylor, C.D., Causey, J.D., Denning, P.D., Hammarstrom, J.M., Hayes, T.S., Horton, J.D., Kirschbaum, M.J., Parks, H.L., Wilson, A.B., Wintzer, N.E., Zientek, M.L., 2013. Descriptive Models, Grade-tonnage Relations, and Databases for the Assessment of Sediment-hosted Copper Deposits - with Emphasis on Deposits in the Central Africa Copperbelt, Democratic Republic of the Congo and Zambia. U.S. Geological Survey Scientific Investigations Report 2010-5090-J, 154 pp. and data files.
Tembo, F., Kampunzu, A.B., Porada, H., 1999. Tholeiitic magmatism associated with continental 677 rifting in the Lufilian Fold Belt of Zambia. J. Afr. Earth Sci. 28, 403–425.
Van Wilderode, J., Debruyne, D., Torremans, K., Elburg, M.A., Vanhaecke, F., Muchez, Ph, 2015. Metal sources for the nkana and konkola stratiform Cu-Co deposits (zambian copperbelt): insights from Sr and Nd isotope ratios. Ore Geol. Rev. 67, 127–138.
Van Wilderode, J., El Desouky, H., Elburg, M., Vanhaecke, F., Muchez, Ph, 2014. Metal sources for the Katanga Copperbelt deposits (DRC): insights from Sr and Nd isotope ratios. Geol. Belg. 17 (2), 137–147.
Van Wilderode, J., Heijlen, W., De Muynck, D., Schneider, J., Vanhaecke, F., Muchez, Ph, 2013. The Kipushi Cu-Zn deposit (DR Congo) and its host rocks: a petrographical, stable isotope (O, C) and radiogenic isotope (Sr, Nd) study. J. Afr. Earth Sci. 79, 143–156.
Wendorff, M., Key, R.M., 2009. The relevance of the sedimentary history of the Grand Conglomerat Formation (Central Africa) to the interpretation of the climate during a major Cryogenian glacial event. Precambrian Res. 172, 127–142.
Young, G.M., 2002. Stratigraphic and tectonic settings of Proterozoic glaciogenic rocks and banded iron-formations: relevance to the snowball Earth debate. J. Afr. Earth Sci. 35, 451–466.
Young, G.M., Nesbitt, H.W., 1999. Paleoclimatology and provenance of the glaciogenic Gowganda Formation (paleoproterozoic), ontario, Canada: a chemostratigraphic approach. Geol. Soc. Am. Bull. 111, 264–274.